SAE 980696

On Multi-axial Random Fatigue Load Modeling

Christoph Leser
MTS Systems Corporation

Lokesh Juneja
EASi Engineering

Surot Thangjitham
Norman E. Dowling
Virginia Polytechnic Institute and State University

ABSTRACT

This study presents a method to achieve a concise description of multidimensional loading histories for fatigue analysis using the stochastic process theory. For purposes of this study, the load history is considered to have stationary random and non-stationary mean and variance content. The stationary variations are represented by a vector Autoregressive Moving Average (ARMA) model while Fourier series are used to model the non-stationary variations.

Justification for this method is provided by comparing the dynamic characteristics of the original loading and reconstruction through their power spectral densities. Further justification is obtained by comparing histograms of principal strain and the corresponding orientation for original loading and reconstruction. Final justification is provided using the resulting fatigue lives of original and simulated loading. To this end, a multi-axial fatigue damage model, valid for approximately proportional loading, is employed and two fatigue failure modes are considered:failure due to normal strain and failure due to shear strain. The shortest predicted life is reported.

A concise description of complex loadings is achieved due to the relatively small number of Fourier coefficients needed and the use of ARMA models. The overall frequency content, correlations, and sequential information of the load history are statistically preserved.

INTRODUCTION

Analytical studies alone cannot provide sufficient information for a fatigue safe design for complex structures because the phenomenon of fatigue failure is still not fully understood. Two methods used for design verification are fatigue testing and simulation studies.

Fatigue testing exposes a structure to the dynamic loads that are anticipated during real operating conditions and records the life to failure. For more effective (and better controlled) testing, it has become customary to perform many fatigue tests in a laboratory rather than in the actual operating environment. As the testing equipment has become more advanced, these laboratory fatigue tests now provide a reliable and efficient way to produce repetitions of complex loadings.

Simulation studies, such as Monte Carlo simulations, are computer-based calculations of the fatigue life according to a structure model and the fatigue phenomenon, including uncertainties with respect to structural and/or loading parameters.

Fatigue loading histories are often lengthy and of random nature; therefore, for both fatigue testing and simulation studies, an efficient description of the loading environment is necessary. Moreover, in many cases multi-axial loading conditions exist, and loading in all directions need to be modeled jointly. The methods for modeling irregular fatigue loadings can be divided into two groups:counting methods and correlation theory based methods (Bílý and Bukoveczky, 1976).

While the counting methods Rainflow Matrix (Matsuishi and Endo, 1968; Dowling, 1972; Perret, 1987; ten Have, 1989) and To-From matrix (Haibach et al., 1976) have been successfully applied to uniaxial loading, no commonly accepted approach has been found to describe multi-axial loadings. This is because closed hysteresis loops cannot be identified for multi-axial loadings. Therefore, correlation theory based methods are employed where the model becomes a substitute for the data and leads to a concise description with few parameters.

A correlation theory based method proposed by Yang (1972) represents the data by its power spectral density (i.e., the frequency domain description of the autocorrelation of the original data). The Markov method, as described by Čačko et al. (1988), falls into this category, as do a more general class of time series called Autoregressive Moving Average (ARMA) models.

Three publications by the authors of this study discuss the use of ARMA models for stationary (Dowling et al., 1992) and non-stationary (Thangjitham et al., 1994 and Leser et al., 1994) one-dimensional fatigue loading histories. Traditionally, ARMA models have been used in the areas of earthquake (Kozin, 1988), wind (Li and Kareem, 1990) and

ocean (Spanos, 1983) engineering to model random load histories. An article reviewing ARMA models for Monte Carlo studies is credited to Spanos and Mignolet (1989).

Random processes can be analyzed either in the time or the frequency domain. Furthermore, random processes can be classified into two categories, stationary and non-stationary. Non-stationary processes have certain characteristics, such as mean or variance, that change over time. The modeling of non-stationarity is important because many real loadings are of non-stationary nature. Time domain analysis techniques are employed because of their efficiency in simulating loadings.

In this study, the modeled history was generated by a ground vehicle traveling on a rough road. This history consists of slowly varying non-stationarities with (respect to mean and variance) and a rapidly varying process-the stationary random variation. To account for such non-stationary variations in an accurate but concise manner, Fourier series are employed because of their versatility when describing loadings and the capability of extending them to a stochastic process. ARMA models are used because of their efficiency in describing stationary random processes, where an ARMA model can be interpreted as a transfer function between a white noise and a general random process.

RANDOM LOAD MODEL

The model developed to describe fatigue random load histories is applicable to both stationary and non-stationary cases, and non-stationarities can be modeled as being either deterministic or stochastic.

ASSUMPTIONS – The time history is a superposition of a zero-mean stationary random process and the events that affect the variation of both the mean and variance. Mean and stationary random components provide distinct contributions to the power spectral density (PSD) of the combined process. The mean variation is slowly varying and contributes only to the low frequency range of the PSD. The stationary random variation however, may affect the PSD at any frequency. The variation in variance, even though it is also assumed to be of slowly varying nature, cannot be detected in a PSD plot of the whole history. It can only be seen if the *evolutionary power spectral density* of the PSD, as a function of time, is known (Priestley, 1965).

Mean and variance variations of each channel are assumed to be independent of the variations of other channels and also independent of stationary random variations. The stationary random variations however, are assumed to be correlated among channels. For the cases studied, random loadings represent actual strain response data at a given point of a vehicle traveling over a rough road. The irregular road profile induces strain, which has a stationary random nature. However, maneuvers such as steering or changing velocity, induce non-stationary variations in strain with respect to mean and variance. The analysis of actual driving behavior (McLean and Hoffmann, 1971) justifies the assumption that driving maneuvers are of slow varying nature.

TIME SERIES MODEL – The following model represents the multi-channel random fatigue loading history with non-stationary mean and variance variation:

$$\mathbf{x}_t = \mathbf{m}_t + \mathbf{s}_t \cdot \mathbf{n}_t$$

(Equation 1)

Where $\mathbf{x}_t = \left[x_t^{(1)} \quad \ldots \quad x_t^{(n)}\right]^T$ represents the underlying history consisting of n channels, $\mathbf{m}_t = \left[m_t^{(1)} \quad \ldots \quad m_t^{(n)}\right]^T$ is the non-stationary variation in the mean value, $\mathbf{s}_t$ is a $(n \times n)$ diagonal matrix with elements $s_t^{(i)}$ as the scaling functions accounting for the variation in variance, and $\mathbf{n}_t = \left[n_t^{(1)} \quad \ldots \quad n_t^{(n)}\right]^T$ a zero-mean stationary random process. The following sections will show how each of the components of Equation 1 are modeled. For simplicity, the derivation will be shown only for the scalar components $m_t^{(i)}$, $s_t^{(i)}$, $n_t^{(i)}$, where the vector and matrix expressions are obtained by combining all n components. Also for convenience, the superscript i will be dropped where it is clear that a component of the vector or matrix is implied. In addition, it is understood that the parameter t refers to discrete points in time, as this study is concerned with modeling evenly sampled time series.

Mean Description - To minimize the number of parameters necessary to characterize the mean variation in a deterministic manner, a truncated Fourier series is used such that:

$$m_t = \frac{1}{2}a_0 + \sum_{k=1}^{M_m}\left[a_k \cos\left(\omega_0 k t \Delta t\right) + b_k \sin\left(\omega_0 k t \Delta t\right)\right]$$

(Equation 2)

Where Δt is the length of the sample interval, $\omega_0 = 2\pi/(N\Delta t)$ is the fundamental frequency, M_m and N are the number of terms in the truncated Fourier series and the total number of sample points of the history, respectively. a_k and b_k are the discrete Fourier coefficients calculated from m_t.

Introducing random phase angles for each term in the summation of Equation 2 allows us to extend the description of the mean as a stochastic process (Rice, 1945). For the case of $M_m \ll (N/2-1)$, m_t approximates the low frequency content of x_t (i.e., its mean variation). The value of M_m is found such that the difference between the original history and truncated Fourier series yields a process, d_t, which is stationary with respect to it's mean, and is expressed as follows:

$$d_t = s_t \cdot n_t = x_t - m_t$$

(Equation 3)

A method for finding the parameter M_m is provided by Buxbaum and Zaschel (1977), who analyze the dynamic system to decide which part of the response spectrum is due to stationary random loadings and non-stationary loadings. Filtering in the frequency domain allows one to separate the two components. However, this is often difficult, as information regarding the dynamic system characteristics and the actual input spectrum are seldom available. Therefore, to determine whether the series d_t is indeed stationary with

respect to its mean value, the methods of nonparametric statistics are used. In essence, according to nonparametric criteria, a series is deemed stationary with respect to it's mean if the variation in the mean is of random nature. More detailed descriptions of this approach can be found in the context of general time series analysis in Bendat and Piersol (1986) and in application to fatigue loadings in Leser (1993), and Leser et al. (1994).

Variance Description - The remaining zero mean component, $s_t \cdot n_t$, must be separated into its respective components. To model the scaling function s_t, in a deterministic manner, a method similar to the one for the mean description is used. The scaling function s_t is defined as the function that renders the quotient d_t / s_t stationary with respect to variance. This is equivalent to saying that s_t is defined as the standard deviation of d_t. In order to estimate the standard deviation of d_t a procedure as shown by Nau et al. (1982) is employed.

For the zero mean time series d_t, sampled at discrete equally spaced intervals, a simple estimate $\tilde{\sigma}_t^2$ for the true variance σ_t^2, is obtained via a moving window such as:

$$\tilde{\sigma}_t^2 = \sum_{j=0}^{n} w_{j-\frac{n}{2}} d_{t+j-\frac{n}{2}}^2$$

(Equation 4)

Where *n* is the width of the window and the window weights, and w_j are such that:

$$\sum_{j=0}^{n} w_{j-\frac{n}{2}} = 1 \qquad w_j \geq 0$$

(Equation 5)

To determine an appropriate size *n* of the window, inference methods from classical statistics can be used. Using a Chi-Square test, a confidence interval can be constructed (Miller and Freund, 1977). For example:

$$\left(\frac{\chi^2_{n-1,1-\alpha}}{n-1} \right) \leq \frac{\tilde{\sigma}_t^2}{\sigma_t^2} \leq \left(\frac{\chi^2_{n-1,\alpha}}{n-1} \right)$$

(Equation 6)

Where σ_t^2 is the value of the true variance, $\tilde{\sigma}_t^2$ is the estimated variance, and $\chi^2_{n-1,\alpha}$ indicates the Chi-Square distribution with $(n-1)$ degrees of freedom at confidence level α. For an acceptable relative maximum error of 25%, the following must hold: $0.75 \leq \tilde{\sigma}_t^2 / \sigma_t^2 \leq 1.25$. Using a Chi-Square distribution table (Miller and Freund, 1977), it can be shown that these bounds, with a chosen value of $\alpha = 0.9$, require a minimum number of $n = 96$. Therefore, a value of $n = 100$ is chosen to estimate the true variance σ_t^2. The quantity $\tilde{\sigma}_t$ then, gives an estimation of the standard deviation of d_t (i.e., an approximation of the scaling function s_t).

The rectangular weighting function is the simplest (i.e., $w_j = 1/(n+1)$). However, a more gradually varying window is generally preferred, such that neighboring points have a stronger influence on the estimate of the variance than points that are further away from the current observation. Nau et al. (1982) uses a cosine bell shaped window. For simplicity, a triangular window is introduced in this study such that:

$$w_j = \begin{cases} \frac{4}{n^2} j & \text{for} \quad 0 \leq j \leq \frac{n}{2} \\ -\frac{4}{n^2} j + \frac{4}{n} & \text{for} \quad \frac{n}{2} \leq j \leq n \end{cases}$$

(Equation 7)

Nau et al. (1982) show that the estimate of the variance using Equation 4 tends to be biased in a systematic way. Peak values in variance will be underestimated, while estimated troughs will be larger than the corresponding true values. A correction can be introduced to account for this known deviation and to obtain a more accurate estimate. However, as a concise (and therefore only approximate) description of the variance is desired, no further refinement is performed.

The next step is to concisely represent the estimated standard deviation $\tilde{\sigma}_t$. The fact that $\tilde{\sigma}_t$ is not evenly distributed makes it difficult to postulate models that would describe it. Therefore, a transformation due to Box and Cox (1964) is commonly used to enhance symmetry:

$$\tilde{\sigma}_t^{BC} = \begin{cases} \tilde{\sigma}_t^{\lambda} & \text{for} \quad \lambda \neq 0 \\ \log \tilde{\sigma}_t & \text{for} \quad \lambda = 0 \end{cases}$$

(Equation 8)

Where $\tilde{\sigma}_t^{BC}$ indicates the Box Cox transform of $\tilde{\sigma}_t$. The parameter λ of this power transformation leads to a logarithmic transformation for $\lambda = 0$ and no transformation for $\lambda = 1$. The parameter λ is chosen such that the transformed series has zero skew (i.e., it becomes symmetrically distributed about it's mean in order to facilitate modeling by a harmonic function). If more than one value of λ fulfills this criterion, the transformed time series corresponding to these values of λ are obtained and their respective mean and variance are calculated. The distribution of the transformed series are compared to normal distributions with the given values of mean and variance for each λ. A normalized error ε, between the frequency histogram of the transformed series and the *probability density function* (pdf) of the corresponding normal distribution is obtained according to Ang and Tang (1975) as:

$$\varepsilon = \sum_{i=1}^{I} \frac{(h_i - f_i)^2}{f_i}$$

(Equation 9)

Where I denotes the number of intervals the total range of $\tilde{\sigma}_t^{BC}$ was divided into, h_i indicates the relative frequency of a certain value of $\tilde{\sigma}_t^{BC}$, and f_i indicates the magnitude of the pdf evaluated at the same value of $\tilde{\sigma}_t^{BC}$. The value of λ that leads to the minimum error, ε, is chosen as the optimal parameter yielding the transformed series that is closest in distribution to a normally distributed process.

In this study, the scaling function s_t, is a truncated Fourier series:

$$s_t^{BC} = \frac{1}{2}c_0 + \sum_{k=1}^{M_s} \left[c_k \cos(\omega_0 kt\Delta t) + d_k \sin(\omega_0 kt\Delta t)\right]$$

(Equation 10)

Where, as before, Δt is the length of the sample interval, $\omega_0 = 2\pi/(N\Delta t)$ is the fundamental frequency, M_s and N are the number of terms in the truncated Fourier series and the total number of sample points of the history, respectively, and c_k and d_k are the discrete Fourier coefficients calculated from $\tilde{\sigma}_t^{BC}$. As for the mean model, introducing random phase angles for each term in the summation of Equation 10 allows us to extend the description of the scaling function to a stochastic process (Rice, 1945). For the limiting case where $M_s = (N/2-1)$, $s_t^{BC} = \tilde{\sigma}_t^{BC}$, while for $M_s < (N/2-1)$, s_t^{BC} is an approximation of $\tilde{\sigma}_t^{BC}$ leading to s_t as a suitable scaling function. The value of M_s is found such that s_t^{BC} and $\tilde{\sigma}_t^{BC}$ have a prescribed correlation coefficient of $\rho_s^{M_s} = 0.95$. Generally, M_s is much smaller than $(N/2-1)$ because the variation in variance has been calculated using an average and is therefore of slowly varying nature.

Random Component Description - The remaining stationary random components, $n_t^{(i)}$, can be represented by an ARMA model of appropriate order. A vector ARMA model is employed to account for correlations among components, $n_t^{(i)}$, of $\mathbf{n}_t$. Estimation of ARMA parameters from observed data may be performed either through maximum likelihood or moment estimators. Both techniques yield efficient, unbiased and consistent estimates. However, the maximum likelihood estimation leads to nonlinear equations with possibly more than one relative maximum (Kay, 1988). The nonlinearities are so severe that the commonly used Newton-Raphson approach will not always converge to a solution (Akaike, 1973). Therefore, approximate procedures in linear form based on the method of moments estimators are often used. Two principal methods coexist using an intermediate approximate model either of pure autoregressive or pure moving average type. These methods, while approximate in nature, will converge to the statistically optimal maximum likelihood estimates given long time series (Kay, 1988).

Using the autocorrelation function of the given data, a large order AR model can be built, which is assumed to be a reliable approximation of the autocorrelation. The autoregressive parameters can be estimated via a system of linear equations. The parameters of the desired ARMA model are obtained by minimizing the difference between the transfer functions of the pure AR model and of the ARMA model. The two stage least square procedure, as introduced by Theil (1958) and applied to ARMA modeling by Durbin (1960), provides the means for the minimization by solving a set of linear equations. Algorithms are described for one dimensional ARMA models by Gersch and Liu (1976) and Gersch and Yonemoto (1977), for multidimensional cases by Samaras et al. (1985), and for modeling random fields by Mignolet and Spanos (1992). The procedure by Samaras et al. (1985) for multi-dimensional ARMA models is chosen in this study for its numerical efficiency. Gersch and Liu (1976) have presented an analogous procedure for single channel estimation. However, the algorithms shown are for the special case where autoregressive and moving average part are of the same order. To allow for more flexible modeling, the method was extended to the general case where both parts may be of different order (Leser, 1993).

No commonly agreed on approach of model order selection for vector ARMA models have been found. For single channel ARMA models some commonly used criteria are *Akaike's Information Criterion, AIC,* (Akaike, 1974), a test based on the *F*-distribution (Pandit,1973), and the so called Q-statistic (Box and Jenkins, 1976). All these tests are based on measuring the statistics of the residuals, i. e. the part of the data not predicted by the model. These methods were applied to time series that contained 50 to 500 observations. For such short records a statistical test will lead to an ARMA model with order p and q well below one hundred, in fact, often below ten. For the case where the observed sequence is much longer, say of order 10^4 to 10^5, however, any statistical test will demand ARMA models of very large order.

Therefore, a new criterion for model order determination is presented that is based on the comparison of the observed time series and the time series obtained from a proposed model. The advantage of this scheme is that a more concise model will be obtained than would be if any of the methods based on residuals is chosen. This is particularly true for the case where one needs to find an ARMA model for a large data set.

After the parameters for a number of ARMA models are estimated, a preliminary selection is made based on the closeness of the auto- and cross- power spectra of a vector ARMA model to the respective spectra of the original loading. A generally applicable measure of association between two variables is provided through the correlation coefficient. For two random variable, *x* and *y*, the correlation coefficient is defined via the covariance, $\mathrm{cov}(x,y)$, and the standard deviations, σ_x and σ_y, as:

$$r_{xy} = \frac{\mathrm{cov}(x,y)}{\sigma_x \sigma_y}$$

(Equation 11)

while an estimator is obtained as:

$$\rho_{xy} = \frac{\sum_{i=1}^{N}(x_i - \bar{x})(y_i - \bar{y})}{\sqrt{\sum_{i=1}^{N}(x_i - \bar{x})^2 \sum_{i=1}^{N}(y_i - \bar{y})^2}}$$

(Equation 12)

Where x_i and y_i are sample points, $\bar{x}$ and $\bar{y}$ are estimators for the mean of the respective variables, and N is the number of sample points. This definition implies that $-1 \le \rho_{xy} \le 1$ and for $\rho_{xy} = 0$ observations of x and y are uncorrelated, while for $\rho_{xy} = 1$ they are identical. In general, the nearer the ρ_{xy} value is to unity, the closer the resemblance between the two.

The closeness of the power spectra, $S_{ij}(f)$, of the original loading to the ones obtained from an ARMA model are therefore measured by their respective correlation coefficients, $\rho_{S_{ij}}^{(p,q)}$. The model with the smallest number of parameters at a given correlation level, e.g. $\rho_{S_{ij}}^{(p,q)} = 0.8$, $\rho_{S_{ij}}^{(p,q)} = 0.9$, etc., is chosen for further study. This allows ruling out a large number of models due to their lack of matching the dynamic characteristics of the original record. The final model selection is based on a comparison of fatigue lives obtained for the original loading and a loading reconstructed using the ARMA model corresponding to a particular correlation level. Unlike the rest of the time series literature, this study ties the step of model building directly to the application of the simulated time series.

MULTI-AXIAL FATIGUE DAMAGE MODEL

The original strain gauge rosette history was obtained from an automotive front suspension component driven through proving ground maneuvers. This history was provided by General Motors Corporation to the Society of Automotive Engineers, Fatigue Design and Evaluation Committee. This set constitutes three channels, where channels 1 and 3 measure strain in directions perpendicular to each other and channel 2 measures strain along a direction which is 45° from both channels 1 and 3. The history, Figure 1, sampled at evenly spaced intervals, assumed to be one second long, containing 12,500 points, constitutes one block.

In order to support the contention that the reconstructed history is equivalent to the original with respect to fatigue life, a simplified multi-axial fatigue damage model for random amplitude loadings was employed (Juneja, 1992). The model requires the applied multi-axial cyclic loading to be approximately proportional. This assumption leads to the choice of a principal strain ratio that is treated as constant for the entire history, which in turn allows the use of deformation plasticity theory to relate stresses and plastic strains. The analysis is conducted by first obtaining the orientation of the critical fatigue damage plane. To assess fatigue life two failure

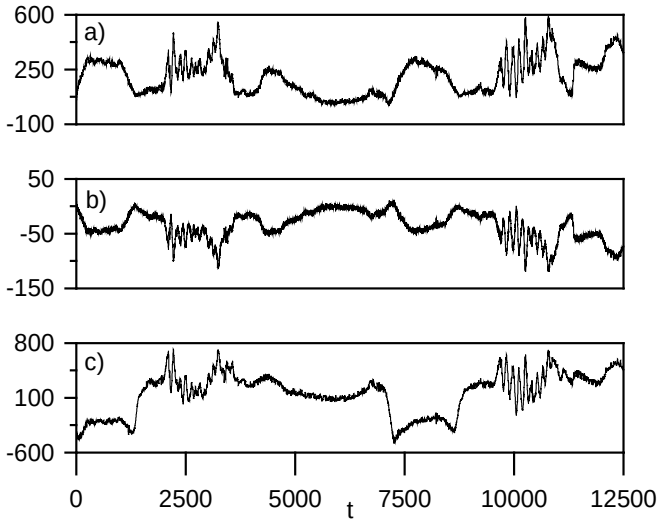

Figure 1.

Time series plots for original history, (a) channel 1, (b) channel 2, and (c) channel 3.

modes are considered. For the first mode, a normal strain based analysis is conducted on the chosen critical plane. Modified versions of Morrow's and the Smith-Watson-Topper mean-stress model are used to incorporate mean-stresses. A second part of the analysis checks for the possibility of shear dominated failure on a critical shear plane.

NORMAL STRAIN BASED ANALYSIS - This section shows the procedure for calculating fatigue life for the case where normal strains lead to failure.

Selection of the Critical Plane - A histogram technique is used in this analysis to choose the critical plane, in which the principal strain values and their corresponding orientations are computed for the entire history. The histogram, as shown for the original loading in Figure 2, is a plot where principal strain orientations with respect to the x-axis of the rosette $(\theta_1 \text{ or } \theta_2)$ appear on the X-axis, while the Y-axis denotes the corresponding principal strain values $(\varepsilon_1 \text{ or } \varepsilon_2)$. For each range of X-Y combinations the number of occurrences are given. This histogram technique was used by Bonnen et al. (1991) to analyze strain rosette data for selecting a critical plane for fatigue life analysis.

Since the counts in the histogram relate to the number of data points in the history for which a particular combination of principal strain values and their orientation occur, the distribution of these counts for a particular principal strain angle indicate the cycling of the strain events for that orientation. For approximately proportional loading, there is not much rotation of principal axes and most of the activity is restricted to one or two directions only. The orientation for which the largest spread of principal strain values is covered, with the most non-zero values in different bins, is chosen to be the critical direction. As observed in Figure 2, most of the cycling of strain events, with significant amplitude, occurs in the region between -45° and -63° (for which the mean is -54°) with respect to the x-axis of the rosette. The crack is expected to initiate and grow under the influence of the strain in this direction, with the strain perpendicular to it having a secondary effect. The strain history is transformed along and perpendicular to this plane, and these are taken to be the new

principal directions, and also the critical direction for fatigue cracking.

ε \ θ	-81	-63	-45	-27	-9	9	27	45	63	81
0.00135	0	0	89	0	0	0	0	0	0	0
0.00121	0	0	115	0	0	0	0	0	0	0
0.00107	0	1	490	0	0	0	0	0	0	0
0.00920	0	17	578	0	0	0	0	0	0	0
0.00780	0	135	755	0	0	0	0	0	0	0
0.00640	0	217	1275	0	0	0	0	0	0	0
0.00500	0	1143	757	6	0	0	0	0	0	0
0.00360	0	1140	731	150	1356	0	0	0	0	0
0.00210	0	679	650	60	627	673	7	0	0	0
0.00070	0	346	102	42	62	282	33	14	0	0
-0.00070	49	2	0	0	0	0	3660	5528	258	78
-0.00210	200	3	0	0	0	0	0	0	0	1883
-0.00360	573	6	0	0	0	0	0	0	0	84
-0.00500	133	11	0	0	0	0	0	0	0	0
-0.00640	0	0	0	0	0	0	0	0	0	0
-0.00780	0	0	0	0	0	0	0	0	0	0
-0.00920	0	0	0	0	0	0	0	0	0	0
-0.01070	0	0	0	0	0	0	0	0	0	0
-0.01210	0	0	0	0	0	0	0	0	0	0
-0.01350	0	0	0	0	0	0	0	0	0	0

Figure 2.

In plane principal strains, ε_1 or ε_2, versus orientation, θ_1 or θ_2, for the original history.

Choice of the Most Damaging Strain Ratio - The principal strain history along the selected critical orientation is analyzed. The in-plane principal strain history perpendicular to this direction is assumed to be always proportional to the history along this direction. Hence, the principal strain ratio that corresponds to the maximum damage needs to be chosen.

Two histograms are computed in order to assist in choosing the principal strain ratio. In one histogram, the ratio of the original principal strains, $\varepsilon_1/\varepsilon_2$, which is obtained from the given strain gage rosette data, is plotted against the corresponding orientations, θ_1 and θ_2. For each ratio, one count corresponding to each principal strain direction is placed. The distribution of the values of the ratio of principal strains for the critical orientation is observed and the most frequently occurring value of the ratio is noted. This histogram for the original loading is shown in Figure 3. You can observe that most of the principal strain ratio values for the orientation range of -45° to -63° (mean -54°) lie at -0.05. Another plot with finer resolution was generated (not shown) and it was observed that most of the strain ratio values lie at –0.08. It is not necessary that the ratio contributing the maximum damage be the same as the noted value from the histogram, since the high count for this value might correspond to large number of small strain amplitude events which do not result in significant damage.

Hence, rainflow cycle counting is performed for the history in order to isolate all the strain amplitude events. A histogram with the ratio of principal strains for each event plotted against the strain range for that event now enables one to look for the ratio that corresponds to the most damaging strain events, where the range is twice the amplitude.

r \ θ	-81	-63	-45	-27	-9	9	27	45	63	81
0.95	0	0	0	0	0	0	0	0	0	0
0.85	0	0	0	0	0	0	0	0	0	0
0.75	0	0	0	0	0	0	0	0	0	0
0.65	0	0	0	0	0	0	0	0	0	0
0.55	0	0	0	0	0	0	0	0	0	0
0.45	0	0	0	0	0	0	0	0	0	0
0.35	0	0	0	0	0	0	0	0	0	0
0.25	0	0	0	0	0	0	0	0	0	0
0.15	0	0	0	0	0	0	0	0	0	0
0.05	0	18	14	0	0	0	0	0	0	0
-0.05	0	3630	4945	18	0	0	0	0	0	0
-0.15	0	30	583	179	0	0	0	0	0	0
-0.25	19	17	0	39	3	0	0	0	0	0
-0.35	243	5	0	17	5	0	0	0	0	0
-0.45	236	0	0	5	28	0	0	0	0	0
-0.55	161	0	0	0	233	0	0	0	0	0
-0.65	145	0	0	0	732	0	0	0	0	0
-0.75	129	0	0	0	580	0	0	0	0	3
-0.85	19	0	0	0	217	0	0	0	0	93
-0.95	3	0	0	0	66	0	0	0	0	85

Figure 3.

Principal strain ratio, *r*,
versus orientation, θ, for the original history.

r \ a^*	0.10	0.31	0.52	0.72	0.93	1.14	1.35	1.55	1.76	1.97
0.57	0	0	0	0	0	0	0	0	0	0
0.51	1	0	0	0	0	0	0	0	0	0
0.45	2	0	0	0	0	0	0	0	0	0
0.39	1	0	0	0	0	0	0	0	0	0
0.33	1	0	0	0	0	0	0	0	0	0
0.27	1	0	0	0	0	0	0	0	0	0
0.21	1	0	0	0	0	0	0	0	0	0
0.15	5	0	0	0	0	0	0	0	0	0
0.09	28	0	0	0	0	0	0	0	0	0
0.03	100	0	0	0	0	0	0	0	0	0
-0.03	517	1	0	0	1	0	0	0	0	0
-0.09	1104	15	7	2	3	2	0	0	0	2
-0.15	98	0	1	0	0	0	1	0	0	0
-0.21	30	0	0	0	0	0	0	0	0	0
-0.27	8	0	0	0	0	0	0	0	0	0
-0.33	5	0	0	0	0	0	0	0	0	0
-0.39	5	0	0	0	0	0	0	0	0	0
-0.45	3	0	0	0	0	0	0	0	0	0
-0.51	2	0	0	0	0	0	0	0	0	0
-0.57	4	0	0	0	0	0	0	0	0	0

*** = 10^{-3}**

Figure 4.

Strain ratio, *r*, versus strain amplitude, *a*,
of the rainflow cycles for the original history.

Figure 4 shows such a histogram for the original loading. It can be seen that most of the strain events (including the major ones) correspond to the strain ratio of -0.09 (which is nearly the same as obtained from the detailed analysis of Figure 3).

State of Stress Effect Modification of Cyclic Stress-Strain Curve - Once the principal strain ratio is selected, the uniaxial cyclic stress-strain curve is modified for the corresponding biaxial state of plane stress. The uniaxial cyclic stress-strain curve for the material is assumed to have the Ramberg-Osgood form

$$\varepsilon_a = \frac{\sigma_a}{E} + \left(\frac{\sigma_a}{H}\right)^{1/n}$$

(Equation 13)

The elastic strains are related to stresses using the *generalized Hooke's law*, while *deformation plasticity theory* is used to relate plastic strains and stresses. Since ε_a and σ_a are related as shown in Equation 13, we have:

$$\bar{\varepsilon}_a = \frac{\bar{\sigma}_a}{E} + \left(\frac{\bar{\sigma}_a}{H}\right)^{1/n}$$

(Equation 14)

where $\bar{\varepsilon}_a$ and $\bar{\sigma}_a$ are effective stress and strain based on octahedral shear stress and strain.

The effective Poisson's ratio, $\bar{\nu}$, is obtained from a chosen point on the effective stress-strain curve of Equation 14 as:

$$\bar{\nu} = \frac{1}{\bar{\varepsilon}_a}\left(0.5\bar{\varepsilon}_{pa} + \frac{\nu\bar{\sigma}_a}{E}\right)$$

(Equation 15)

Where ν is the elastic Poisson's ratio, and the subscript p refers to plastic strain. This value of $\bar{\nu}$, and the selected principal strain amplitude ratio value (see the section on Choice of the Most Damaging Strain Ratio), allow the calculation of the principal stress amplitude ratio for the chosen point on the effective stress-strain curve. Details follow.

For plane stress conditions, the strain amplitude in the principal direction 1 is obtained by adding elastic and plastic parts using deformation plasticity theory, which gives:

$$\varepsilon_{1a} = \frac{1}{E_t}\left(\sigma_{1a} - \bar{\nu}\sigma_{2a}\right)$$

(Equation 16)

Where the subscript 1 indicates the principal direction and $E_t = \bar{\sigma}_a/\bar{\varepsilon}_a$ is the secant modulus on the effective stress-strain curve. Similarly, for principal direction 2:

$$\varepsilon_{2a} = \frac{1}{E_t}\left(\sigma_{2a} - \bar{\nu}\sigma_{1a}\right)$$

(Equation 17)

From equations 16 and 17 we get the principal stress amplitude ratio, λ:

$$\lambda = \frac{\sigma_{2a}}{\sigma_{1a}} = \frac{\bar{\nu} + \left(\varepsilon_{2a}/\varepsilon_{1a}\right)}{1 + \bar{\nu}\left(\varepsilon_{2a}/\varepsilon_{1a}\right)}$$

(Equation 18)

Stress and strain amplitudes in the principal direction 1 are the found using the following equations:

$$\sigma_{1a} = \frac{\bar{\sigma}_a}{\sqrt{1 - \lambda + \lambda^2}}$$

(Equation 19)

$$\varepsilon_{1a} = \frac{1 - \bar{\nu}\lambda}{\sqrt{1 - \lambda + \lambda^2}}\bar{\varepsilon}_a$$

(Equation 20)

Equations 16 through 20 are adapted from Hoffmann et al. (1985a, 1985b).

Constants, defining the new curve, are fit to the σ_{1a} and ε_{1a} values obtained for the various points. The new curve is assumed to also have the Ramberg-Osgood form:

$$\varepsilon_{1a} = \frac{\sigma_{1a}}{E_n} + \left(\frac{\sigma_{1a}}{H_n}\right)^{1/n_n}$$

(Equation 21)

Where, E_n, H_n, and n_n are new fitting constants. The new Young's modulus, E_n, is fitted using the elastic case, for which $\bar{\nu} = \nu$ and $\bar{\sigma}_a/\bar{\varepsilon}_a = E$. Hence, we get:

$$E_n = \frac{\sigma_{1a}}{\varepsilon_{1a}} = \frac{E}{1 - \nu\lambda}$$

(Equation 22)

Stress-Strain Modeling: Hysteresis Loop Curves

Rainflow cycle counting is performed on the strain history along the critical plane, revealing that the transformed record of the original loading contains 1965 major peaks and valleys. This is done in order to isolate each cycle in the history and to obtain the strain amplitude for that cycle.

To perform rainflow cycle counting, the order of the history is arranged so that the largest peak is first in the history. The history is first filtered to obtain peaks and valleys only, omitting all intermediate points. A peak-valley-peak or valley-peak-valley is considered to be a cycle if the second strain range is greater than the first. Each time a cycle is counted, the appropriate peaks are removed from the history and the corresponding cycle is recorded. The complete set of rules for performing rainflow cycle counting is described in ASTM (1996).

The stress for the first peak, which is the largest peak in the history, is determined using the monotonic stress-strain curve. For unloading following the largest peak, and for further cyclic loading, it is suggested by the rheological models that yielding should occur if the strain range exceeds twice the yield strain from the monotonic stress-strain curve. Hence, for these situations, the hysteresis loop path is predicted by the curve obtained by a factor of two expansion of the monotonic stress-strain curve:

$$\frac{\Delta\varepsilon}{2} = f\left(\frac{\Delta\sigma}{2}\right)$$

(Equation 23)

or,

$$\frac{\Delta\varepsilon}{2} = \frac{\Delta\sigma}{2E} + \left(\frac{\Delta\sigma}{2H}\right)^{1/n}$$

(Equation 24)

For Equation 24, $\Delta\sigma$ and $\Delta\varepsilon$ are measured from an origin which is the point where the loading directions change. Hence, this origin shifts its position continually to the next recent point of direction change. In addition, the stress-strain behavior exhibits a memory effect after completion of a loop, i.e., it returns to the path previously established. (This fairly standard stress-strain modeling procedure is described in Chapter 12 of Dowling (1993) and elsewhere.)

Modulus of Elasticity, E	202000 MPa	29297 ksi
Yield Strength, σ_Y	380 MPa	55.1 ksi
Ultimate Strength, σ_U	6321 MPa	90.3 ksi
Fatigue Strength Coefficient, σ'_f	948 MPa	138 ksi
Cyclic Strength Coefficient, H'	1258 MPa	182 ksi
Cyclic Strain Hardening Exponent, n'	0.208	
Fatigue Strength Exponent, b	-0.092	
Fatigue Ductility Coefficient, ε'_f	0.260	
Fatigue Ductility Exponent, c	-0.445	

Table 1.

Material properties for SAE 1045 steel, Kurath et al. (1989).

Life Calculations - All fatigue life calculations are based on the material properties of SAE 1045 steel, stated in Table 1. Two mean stress models, that of Morrow, and that of Smith, Watson, and Topper, modified for the multiaxial loading, are used to incorporate mean-stresses into the life calculations.

For the Morrow model, the effective strain amplitude is chosen to be the damage parameter used to relate the multiaxial strain history to the uniaxial life equation; hence, the life is postulated to depend on the effective strain amplitude. The life equation for the biaxial state of stress $(\sigma_{3a} = 0, \sigma_{2a} = \lambda\sigma_{1a})$, with the effective strain amplitude as the damage parameter, is obtained by adding the elastic and plastic parts of strain using deformation plasticity theory:

$$\varepsilon_{1a} = \frac{\sigma'_f}{E}\frac{1-\nu\lambda}{\sqrt{1-\lambda+\lambda^2}}(2N)^b + \varepsilon'_f\frac{1-0.5\lambda}{\sqrt{1-\lambda+\lambda^2}}(2N)^c$$

(Equation 25)

Where the uniaxial strain life curve generated from tensile testing is used to derive Equation 25 and the constants are b (elastic) stress life exponent and c plastic strain life exponent.

The modified version of the Morrow mean stress model leads to:

$$N_f = N\Big/\left(1-\overline{\sigma}_m\Big/\sigma'_{f_{eff}}\right)^{1/b}$$

(Equation 26)

In which N_f is the mean modified number of cycles to failure $\overline{\sigma}_m = \sigma_{m1} + \sigma_{m2} + \sigma_{m3}$ and $\sigma'_{f_{eff}} = \sigma'_f(1-\nu\lambda)\Big/\sqrt{1-\lambda+\lambda^2}$. Where σ_{m1}, σ_{m2}, and σ_{m3} are the mean stresses in the principal directions 1, 2, and 3 respectively. Equations 25 and 26 are adapted from Chapter 14 Dowling (1993).

The Smith-Watson-Topper model for mean stresses is used with the principal strain history along the critical orientation, which is considered to be related to life. In particular, the principal strain amplitude is coupled with the maximum stress on the critical plane to incorporate mean stress effects. The equation describing this model is:

$$\sigma_{\max}\frac{\Delta\varepsilon_1}{2} = \sigma'_f\varepsilon'_f(2N_f)^{b+c} + \frac{\sigma'^2_f}{E}(2N_f)^{2b}$$

(Equation 27)

Where the right hand side is based on the uniaxial strain life curve generated from completely reversed controlled strain testing.

A linear damage rule, known as the Palmgren-Miner rule (Palmgren (1945), Miner (1945)) is used with either Equation 26 or 27 to find the life in terms of blocks (repetitions of history) to failure. To employ the Palmgren-Miner rule, the number of cycles, n_i, applied at strain amplitude ε_i is divided by the cycles to failure, $N_i = N_f$, corresponding to ε_i, to obtain the life fraction, n_i/N_i. Failure is reached when the sum of life fractions for the various strain cycles equals unity.

$$\sum_i \frac{n_i}{N_i} = 1$$

(Equation 28)

MAXIMUM SHEAR STRAIN BASED ANALYSIS - This analysis is conducted in order to check for shear strain dominated damage on the critical plane. The most damaging maximum shear strain on the critical plane is chosen by considering both the in-plane and the out-of-plane shear strains.

The maximum shear strain amplitude coupled with the tensile stress perpendicular to the plane of maximum shear strain is considered to be the damage parameter in the strain life equation. The model, which also incorporates mean-stress

effects, is described by the following equation:

$$\gamma_{\max}\left(1+\frac{\sigma_n}{\sigma_y}\right)=\gamma'_f\left(2N_f\right)^c+\frac{\tau'_f}{G}\left(2N_f\right)^b$$

(Equation 29)

Where $\gamma_{\max}$ is the maximum shear strain amplitude, σ_n is the maximum tensile stress perpendicular to the maximum shear strain plane during the cycle, σ_y is the yield strength, G is the shear modulus, γ'_f is the shear fatigue ductility coefficient, τ'_f is the shear fatigue strength coefficient. This model was proposed by Socie (1987). He considers the minimum of the life obtained by this model and by the Smith-Watson-Topper model (Equation 27) to be the controlling value of life, where the former predicts tensile mode cracking and the latter, shear mode cracking. The right hand side of Equation 29 is the description of the strain-life curve generated from torsion testing, the constants for which can be estimated from tensile material constants using the expression given by Socie (1987), i.e., $\gamma'_f=1.66\varepsilon'_f$, $\tau'_f/G=1.44\sigma'_f/E$ and $G=E/2(1+\nu)$. The life is obtained in terms of blocks to failure (repetitions of the history) using cycle counting and the Palmgren-Miner rule, as described before.

The minimum of all three life estimates, i.e. Morrow (eqs. 25-26), Smith-Watson-Topper (eq. 27), and shear strain (eq.29), is considered to be the final estimate. A number of scaling factors are applied to the input strain history in order to obtain a strain life diagram where the fatigue life, as a function of the input strain levels, is shown. The fatigue life is then calculated for each scaling factor.

RESULTS AND DISCUSSION

According to the employed model of Equation 1, the history is decomposed into its three components: the mean component $\mathbf{m}_t$, the scaling function $\mathbf{s}_t$, and the stationary random part $\mathbf{n}_t$. Where it is understood that the three channels (such as $m_t^{(1)}$, $m_t^{(2)}$, and $m_t^{(3)}$) constitute the respective vector $\mathbf{m}_t$ and will from now on be referred to as $m_t^{(i)}$. In order to model the variation of the mean $m_t^{(i)}$ in a deterministic way, various Fourier series with increasing numbers of terms are formed, giving the tentative mean descriptions. The difference of the original records and each mean description $x_t^{(i)}-m_t^{(i)}=n_t^{(i)}\cdot s_t^{(i)}$ are obtained. These differences are then analyzed for deviations from being a zero-mean process. The best (most concise) mean description is chosen as the one that renders $n_t^{(i)}\cdot s_t^{(i)}$ stationary, with respect to its mean, using the Fourier series with the least number of terms.

Nonparametric run tests were performed and it was seen that for all channels (1, 2, and 3), a value of $M_m=50$ renders the series $n_t^{(i)}\cdot s_t^{(i)}$ stationary (with respect to their mean) although only approximately so for channel 3. See Fig. 5b for the deterministic mean Model $m_t^{(1)}$ and Fig. 5c for the mean removed record $n_t^{(1)}\cdot s_t^{(1)}$ for one channel of the rosette data.

In order to model the scaling functions $s_t^{(i)}$, an estimate of the standard deviation of the time series $\tilde{\sigma}_t^{(i)}$ is obtained according to Equation 4 (shown in Fig. 5d). For a concise representation of $\tilde{\sigma}_t^{(i)}$, the Box-Cox transformations are performed (where $\lambda^{(1)}=-0.613$, $\lambda^{(2)}=-1.318$, and $\lambda^{(3)}=-0.524$ are the optimal transformation parameters) and the transformed series $\tilde{\sigma}_t^{(1)BC}$ is shown in Fig. 5e. A number of Fourier series (with an increasing number of terms) are formed according to Equation 10, giving the tentative scaling functions.

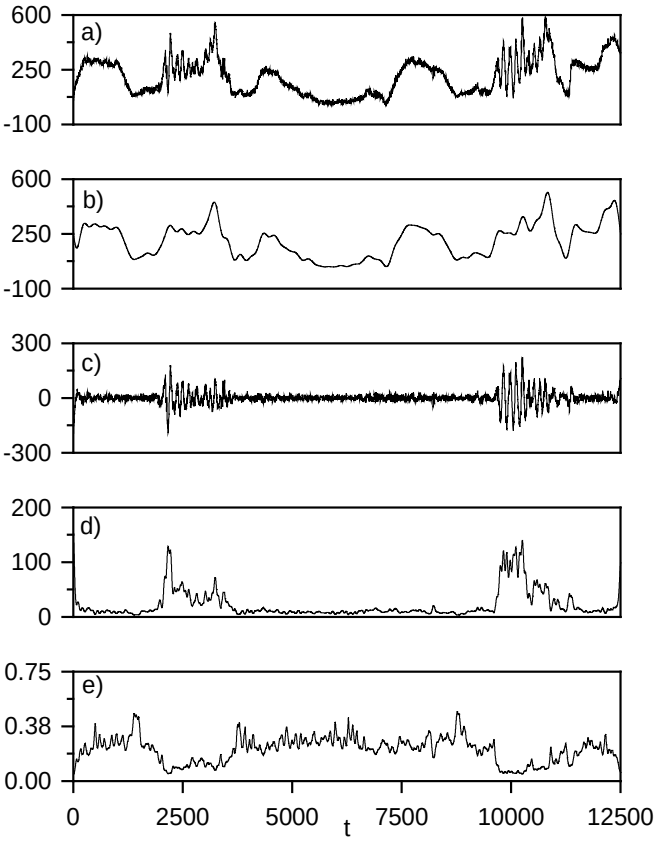

Figure 5.

Time series plots for (a) original history, (b) deterministic mean with $M_\mu=50$, (c) mean-removed series, (d) estimated standard deviation, $\tilde{\sigma}_t$, and (e) Box-Cox transformation of $\tilde{\sigma}_t$, $\tilde{\sigma}_t^{BC}$ for channel 1.

The series with the fewest number of terms that are correlated at 95% to $\tilde{\sigma}_t^{(i)BC}$ (denoted $s_t^{(i)BC}$) has $M_s=40$ terms for channel 1, $M_s=90$ terms for channel 2, and $M_s=80$ terms for channel 3. This series for channel 1 is shown in Fig. 6a. The inverse Box-Cox transformation of $s_t^{(i)BC}$ (denoted $s_t^{(i)}$) is the scaling function used to render the mean-removed series $n_t^{(i)}\cdot s_t^{(i)}$ stationary, with respect to

variance (one of which is shown in Fig. 6b). The stationary series, i.e. $n_t^{(1)}$ is shown in Fig. 6c.

The stationary series are represented by a three-dimensional ARMA model. Parameters for a number of ARMA models are estimated and the correlation coefficient between power spectra of these ARMA models and the spectra of the stationary series are calculated; see Table 2. Because the auto- and cross-spectra of the stationary are relatively simple, low order ARMA models fit these spectra well. Therefore, models are sought where all of the spectra, $S^{(ij)}(f)$ have a minimum correlation of $\rho_{S^{(ij)}}^{(p,q)}$ greater than 0.9, 0.95, 0.97, 0.98 to the respective spectra obtained for the stationary series. This leads to the choice of ARMA(2,0), ARMA(2,1), ARMA(3,0), and ARMA(6,5). It is noted that increasing the model order beyond ARMA(6,5) does not increase the correlation coefficients. One auto- and one cross-spectral density for ARMA(2,0) and ARMA(6,5) are shown in Figs. 7 and 8. The area under the spectral densities is well approximated by both models, but the higher order model fits the peaks better. Moreover, as both spectra are shown on a logarithmic scale, the agreement is actually quite good as can be seen by the very close fit in the low frequency range, where the largest portion of the power of the process is concentrated.

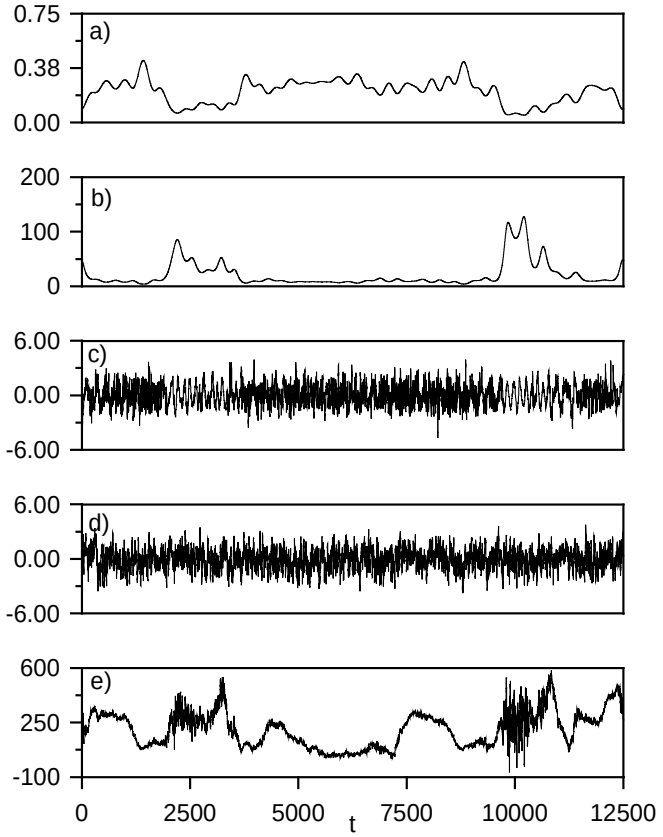

Figure 6.

Time series plots for (a) Fourier series approximation to $\tilde{\sigma}_t^{BC}$ with $M_s = 40$, s_t^{BC}, (b) scaling function, s_t, (c) stationary series, (d) ARMA(6,5) model simulation, and (e) reconstruction for channel 1.

p \ q	0	1	2	3	4	5	6	7
1	0.86_{13}							
2	$\mathbf{0.93_{22}}$	$\mathbf{0.96_{22}}$						
3	$\mathbf{0.97_{22}}$	0.97_{22}	0.97_{22}					
4	0.96_{22}	0.96_{22}	0.97_{22}	0.96_{13}				
5	0.95_{13}	0.96_{13}	0.96_{13}	0.97_{33}	0.88_{33}			
6	0.95_{22}	0.95_{22}	0.95_{33}	0.94_{22}	0.86_{13}	$\mathbf{0.98_{33}}$		
7	0.97_{22}	0.97_{22}	0.97_{22}	0.97_{33}	0.86_{13}	0.88_{33}	0.97_{11}	
8	0.94_{22}	0.94_{22}	0.94_{22}	0.96_{22}	0.86_{13}	0.88_{33}	0.98_{22}	0.97_{22}

Table 2.

Correlation coefficient of power spectra, $\rho_{S_{ij}}^{(p,q)}$, for selected ARMA(*p*,*q*) models, where the subscript indicates the auto- or cross-spectrum with minimal correlation coefficient and the bold number indicates the minimum order model for a given correlation value.

Time series are generated for all ARMA models, as in Fig. 6d for channel 1, are multiplied by the deterministic scaling functions, $s_t^{(i)}$, and then are added to the deterministic mean variations, $m_t^{(i)}$. A complete reconstruction, using a realization of the selected ARMA(6,5) model is shown in Fig. 6e for channel 1 and in Fig. 9 for all three channels. It is noted that the original time series for all three channels exhibit, in the region of t=2500 and t=10000, a distinctly different pattern. It is presumed that a maneuver was executed that included a few large amplitude short duration (spike) events. The spectral content of this part of the series is therefore distinctly different from the remaining series. Consequently, the reconstruction will perform poorly in that region. It can be seen in the reconstruction that for these regions a much larger number of large amplitude cycles are predicted than were present in the original loading. This will affect fatigue life predictions.

The power spectral densities, $S^{(ij)}(f)$, of the original and reconstructed histories are shown in Figs. 10 and 11. As the spectra are calculated for the record as a whole, any of the above stated variations in spectral content, as they are of short duration, are averaged and cannot be observed.

The same histograms as shown for the original record were obtained for the reconstructed history. Figures 12 through 14 show that the reconstruction displays the same kind of proportionality as the original record and that most of the cycling activity is in one direction. Namely, the critical angle is again observed to be approximately -54° (Fig. 12, the mean of the range from -45° to -63°) and the most damaging strain ratio is about -0.05 (Fig. 13). Moreover, a rainflow cycle count of the transformed history reveals 2136 cycles, compared to 1965 for the original history. All fatigue relevant characteristics, therefore, are well reproduced by the reconstructed history.

The strain life curves for SAE 1045 steel are calculated according to the simplified critical plane approach

described in the section on Multiaxial Fatigue Damage Model, and are shown in Fig. 15. The failure mode, i.e. the minimal fatigue life as predicted by Morrow, Smith-Watson-Topper, and shear strain was different across the range of scaling factors. Reconstructions using ARMA(2,0), ARMA(2,1), ARMA(3,0), and ARMA(6,5) models predict fatigue lives that are very close to the others, such that strain life curves partially overlap. Consequently, only the prediction for ARMA(6,5) is shown. The ARMA(0,0) and ARMA(1,0) models constitute the limiting cases on fatigue life as they fall well below and above the life of the ARMA(6,5) reconstruction. Because the reconstruction introduced a number of large cycles that are not present in the original loading, all reconstructions tend to be biased toward shorter lives. In fact, the limiting case of the ARMA(1,0) reconstruction that predicts the longest life is the one that is closest to the life predicted for the original record. However, of all reconstructions with a minimum correlation for the power spectra, $\rho_{S^{(ij)}}^{(p,q)} \geq 0.9$, the strain life curve obtained from the ARMA(6,5) model was closest to the one obtained from the original loading. The ARMA(6,5) model was, therefore, deemed appropriate for reconstruction as both spectral shape and fatigue life agreed reasonably well with the original.

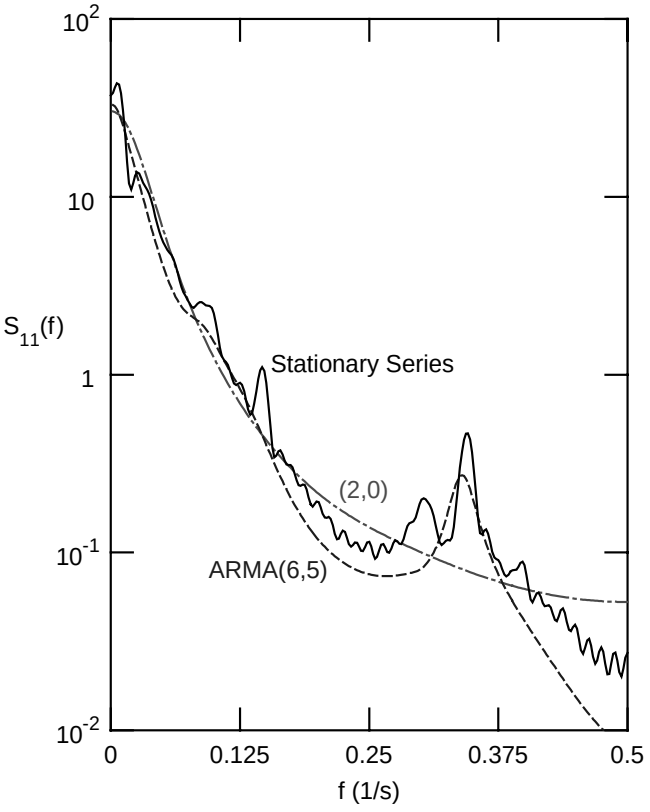

Figure 7.

Power spectral density, $S_{11}(f)$, for the stationary series, for ARMA(2,0) with $\rho_{S_{33}}^{(2,0)} = 0.93$, and for ARMA(6,5) with $\rho_{S_{22}}^{(6,5)} = 0.98$.

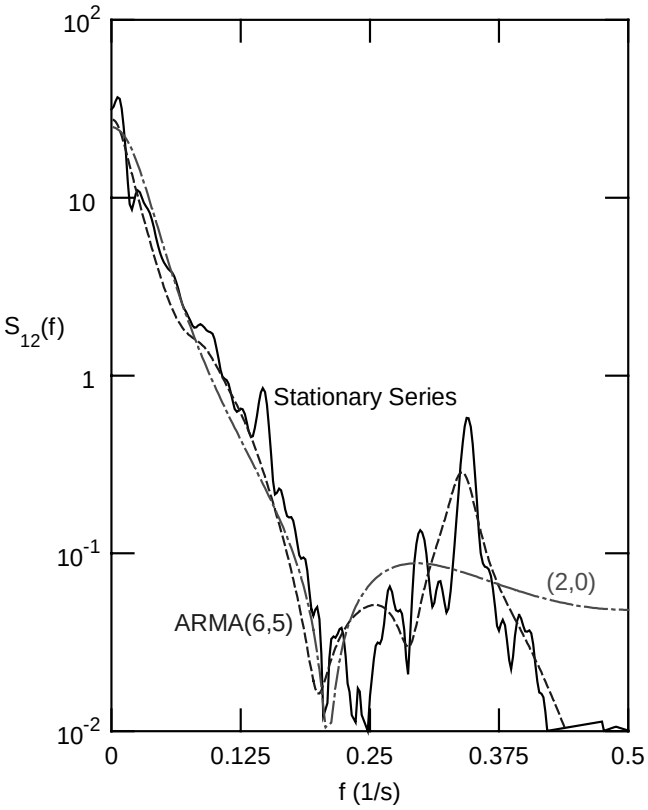

Figure 8.

Power spectral density, $S_{12}(f)$, for the stationary series, for ARMA(2,0) with $\rho_{S_{33}}^{(2,0)} = 0.93$, and for ARMA(6,5) with $\rho_{S_{22}}^{(6,5)} = 0.98$.

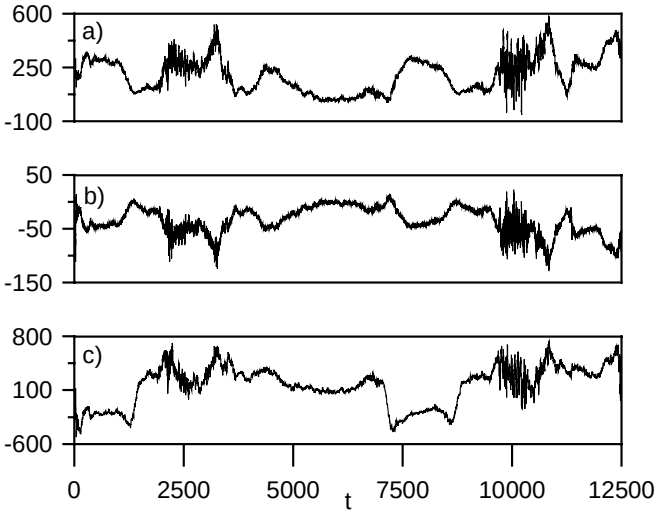

Figure 9.

Time series plots for reconstructed history.

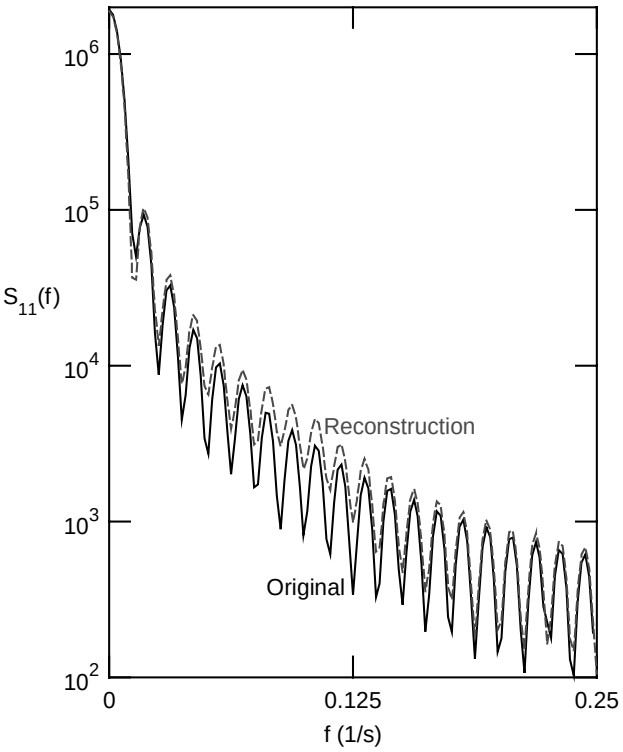

Figure 10.

Power spectral density, $S_{11}(f)$, for the original history and a reconstructed history.

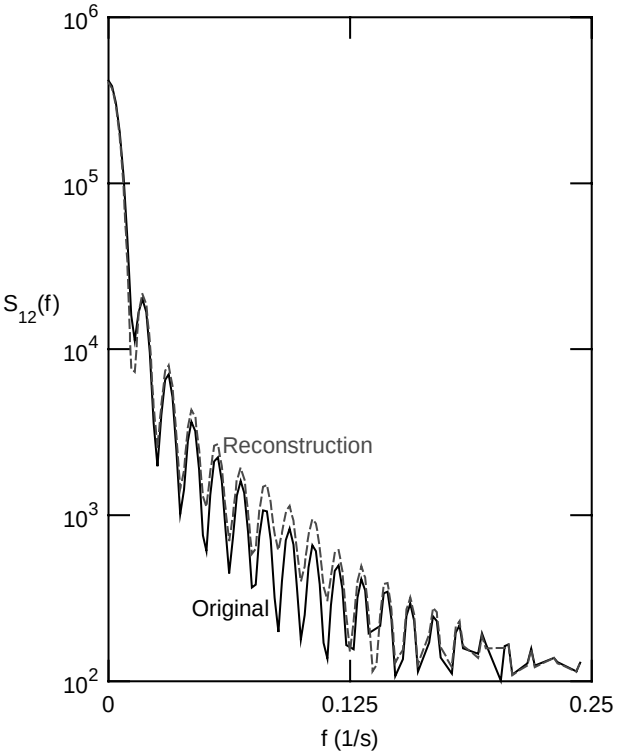

Figure 11.

Power spectral density, $S_{12}(f)$,
for the original history and a reconstructed history.

ε \ θ	-81	-63	-45	-27	-9	9	27	45	63	81
0.00135	0	0	40	0	0	0	0	0	0	0
0.00121	0	1	242	0	0	0	0	0	0	0
0.00107	0	24	315	0	0	0	0	0	0	0
0.00920	0	50	547	0	0	0	0	0	0	0
0.00780	0	143	757	1	0	0	0	0	0	0
0.00640	0	286	1387	4	0	0	0	0	0	0
0.00500	0	1060	850	22	0	0	0	0	0	0
0.00360	0	1145	664	121	1428	0	0	0	0	0
0.00210	0	573	635	43	621	615	0	0	0	0
0.00070	0	299	171	62	67	290	60	26	1	0
-0.00070	59	1	0	0	0	0	3558	5581	252	93
-0.00210	164	13	0	0	0	0	0	1	0	1940
-0.00360	515	22	0	0	0	0	0	0	0	83
-0.00500	146	1	0	0	0	0	0	0	0	0
-0.00640	21	0	0	0	0	0	0	0	0	0
-0.00780	0	0	0	0	0	0	0	0	0	0
-0.00920	0	0	0	0	0	0	0	0	0	0
-0.01070	0	0	0	0	0	0	0	0	0	0
-0.01210	0	0	0	0	0	0	0	0	0	0
-0.01350	0	0	0	0	0	0	0	0	0	0

Figure 12.

In plane principal strains, ε_1 or ε_2, versus orientation, θ_1 or θ_2, for the reconstructed history.

r \ θ	-81	-63	-45	-27	-9	9	27	45	63	81
0.00135	0	0	0	0	0	0	0	0	0	0
0.00121	0	0	0	0	0	0	0	0	0	0
0.00107	0	0	0	0	0	0	0	0	0	0
0.00920	0	0	0	0	0	0	0	0	0	0
0.00780	0	0	0	0	0	0	0	0	0	0
0.00640	0	0	0	0	0	0	0	0	0	0
0.00500	0	0	0	0	0	0	0	0	0	0
0.00360	0	0	0	0	0	0	0	0	0	0
0.00210	0	0	0	0	0	0	0	0	0	0
0.00070	0	23	26	1	0	0	0	0	0	0
-0.00070	0	3449	4830	38	0	0	0	0	0	0
-0.00210	0	115	749	107	1	0	0	0	0	0
-0.00360	25	28	3	75	7	0	0	0	0	0
-0.00500	197	3	0	22	8	0	0	0	0	0
-0.00640	277	0	0	10	29	0	0	0	0	0
-0.00780	147	0	0	0	168	0	0	0	0	0
-0.00920	141	0	0	0	807	0	0	0	0	0
-0.01070	87	0	0	0	595	0	0	0	0	1
-0.01210	18	0	0	0	197	1	0	0	0	75
-0.01350	9	0	0	0	105	3	0	0	0	123

Figure 13.

Principal strain ratio, *r*, versus orientation, θ,
for the reconstructed history.

r \ a*	0.10	0.31	0.52	0.72	0.93	1.14	1.35	1.55	1.76	1.97
0.57	0	0	0	0	0	0	0	0	0	0
0.51	0	0	0	0	0	0	0	0	0	0
0.45	3	0	0	0	0	0	0	0	0	0
0.39	2	0	0	0	0	0	0	0	0	0
0.33	0	0	0	0	0	0	0	0	0	0
0.27	3	0	0	0	0	0	0	0	0	0
0.21	3	0	0	0	0	0	0	0	0	0
0.15	13	0	0	0	0	0	0	0	0	0
0.09	25	0	0	0	1	0	0	0	0	0
0.03	98	0	0	0	0	0	0	0	0	0
-0.03	493	6	1	1	0	0	0	1	0	0
-0.09	1209	42	17	4	4	1	0	1	1	1
-0.15	107	0	1	1	0	1	0	0	0	0
-0.21	21	0	0	0	0	0	0	0	0	0
-0.27	11	0	0	2	0	0	0	0	0	0
-0.33	9	0	0	0	1	0	0	0	0	0
-0.39	6	0	0	0	0	0	0	0	0	0
-0.45	5	0	0	0	0	0	0	0	0	0
-0.51	4	0	0	0	0	0	0	0	0	0
-0.57	1	0	0	0	0	0	0	0	0	0

*** = 10^{-3}**

Figure 14.

Strain ratio, *r*, versus strain amplitude, *a*, of the rainflow cycles for the reconstructed history.

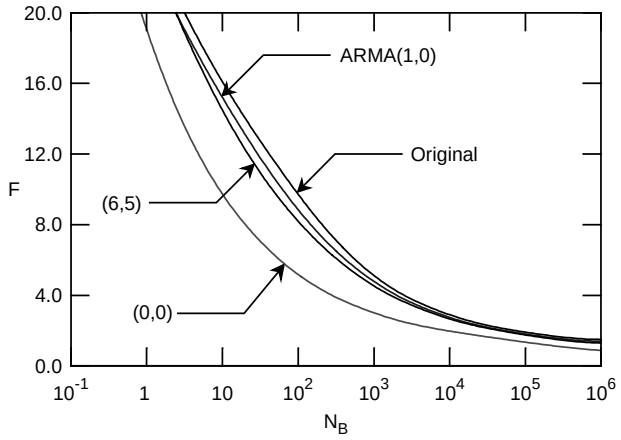

Figure 15.

Scaling factor, *F*, versus blocks to failure, N_B, for the original and selected ARMA reconstructed histories.

SUMMARY

The method for loading descriptions (shown above) was developed in the framework of vehicle loadings. However, it can generally be used for any application where lengthy random loadings need to be presented in a concise manner. The simplified fatigue model can be applied to any structure under complex loadings when the phase relationship among load directions is approximately constant. Both the loading description and fatigue damage assessment allow for an analysis of the structures' weakest points prior to testing.

ACKNOWLEDGMENTS

This work was supported by MTS Systems Corporation, Minneapolis, MN. The support is greatly appreciated. The technical monitors were James W. Fash and Phil E. Grote.

REFERENCES

1. Akaike, H., "Maximum Likelihood Identification of Gaussian Autoregressive Moving Average Models", *Biometrika*, Vol. 60, No. 2, 1973, pp. 255-265.
2. Akaike, H., "A New Look at the Statistical Model Identification", *IEEE Transactions on Automatic Control*, Vol. AC-19, No. 6, Dec., 1974, pp. 716-723.
3. Ang, A. H-S., and Tang, W. H., *Probability Concepts in Engineering Planning and Design*, Vol. 1, John Wiley & Sons, New York, 1975.
4. ASTM, "Standard Practices for Cycle Counting in Fatigue Analysis," *Annual Book of ASTM Standards*, Vol. 03.01, American Society for Testing and Materials, Philadelphia, PA, Standard No. E 1045, 1996.
5. Bendat, J. S. and Piersol, A. G., *Random Data: Analysis and Measurement Procedures*, Second Edition, Wiley-Interscience, New York, 1986.
6. Bílý, M., Bukoveczky, J., "Digital Simulation of Environmental Processes with Respect to Fatigue," *Journal of Sound and Vibration*, Vol. 49, No. 4, 1976, pp. 551-568.
7. Bonnen, J. J., Conle, F. A., and Chu, C. C., "Biaxial Torsion-Bending Fatigue of SAE Axle Shafts," *Society of Automotive Engineers*, Warrendale, PA, No. 910164, 1991.
8. Box, G. E. P. and Cox, D. R., "An Analysis of Transformation," *Journal of the Royal Statistical Society*, Series B, Vol. 26, 1964, pp. 211-252.
9. Box, G. E. P. and Jenkins, G. M., *Time Series Analysis Forecasting and Control*, second edition, Holden-Day, San Francisco, 1976.
10. Buxbaum, O. and Zaschel, J. M., "Beschreibung stochastischer Beanspruchungs-Zeit-Funktionen: Description of stochastic Loading Time Series," *Fraunhofer-Gesellschaft, Laboratorium für Betriebsfestigkeit*, Darmstadt, LBF FhG Report, No. FB-140, 1977.
11. Čačko, J., Bílý, M. and Bukoveczky, J., *Random Processes: Measurement, Analysis and Simulation*, Elsevier, Amsterdam, 1988.
12. Dowling, N. E., "Fatigue Failure Predictions for Complicated Stress-Strain Histories," *Journal of Materials*, Vol. 7, No. 1, 1972, pp. 71-87.
13. Dowling, N. E., Thangjitham, S., Leser, C. and Fash, J. W., "Some comments on Methods of Reducing and Reconstructing Irregular Fatigue Loading Histories," pp. 52-61, *The Rainflow Method in Fatigue*, Y. Murakami, ed., Butterworth-Heinemannn, Oxford, 1992.
14. Dowling, N. E., *Mechanical Behavior of Materials*, Prentice Hall, Englewood Cliffs, 1993.
15. Durbin, H., "The Fitting of Time Series Models," *Reviews of the Institute of International Statistics*, Vol. 28, 1960, pp. 233-243.
16. Gersch, W. and Liu, R. S-Z., "Time Series Methods for the Synthesis of Random Vibration Systems," *Journal of Applied Mechanics*, Vol. 98, Mar., 1976, pp. 159-165.
17. Gersch, W. and Yonemoto, J., "Synthesis of Multivariate Random Vibration Systems: A Two-Stage Least Square AR-MA Model Approach," *Journal of Sound and Vibration*, Vol. 52, No. 4, 1977, pp. 553-565.
18. Haibach, E., Fischer, R., Schütz, W. and Hück, M., "A Standard Random Load Sequence of Gaussian Type Recommended for General Application in Fatigue Testing; Its Mathematical Background and Digital Generation," *Fatigue Testing and Design*, Vol. 2, S.E.E. International Conference,

London, 5 - 9 April, 1976, pp. 29.1-29.21.
19. Hoffmann, M. and Seeger, T., "A Generalized Method for Estimating Multiaxial Elastic-Plastic Notch Stresses and Strains Part 1: Theory," *Journal of Engineering Materials and Technology*, Vol. 107, Oct., 1985, pp. 250-254.
20. Hoffmann, M. and Seeger, T., "A Generalized Method for Estimating Multiaxial Elastic-Plastic Notch Stresses and Strains Part 2: Application and General Discussion," *Journal of Engineering Materials and Technology*, Vol. 107, Oct., 1985, pp. 255-260.
21. Juneja, L. K., *Multiaxial Fatigue Damage Model for Random Amplitude Loading Histories*, M.S. Thesis, Dept. of Engineering Science and Mechanics, Virginia Polytechnic Institute and State University, 1992.
22. Kay, S. M., *Modern Spectral Estimation: Theory and Application*, Prentice Hall, Inc., Englewood Cliffs, 1988.
23. Kozin, F., "Autoregressive Moving Average Models of Earthquake Records," *Probabilistic Engineering Mechanics*, Vol. 3, No. 2, 1988, pp. 58-63.
24. Kurath, P., Downing, S. D., and Galliart, D., "Chapter 2: Summary of Non-Hardened Shaft Round Robin Program", G. E. Leese and D. F. Socie, eds., *Multiaxial Fatigue: Analysis and Experiments*, Society of Automotive Engineers, Warrendale, PA, Vol. AE-14, 1989, pp. 13-31.
25. Leser, C., *On Stationary and Nonstationary Fatigue Load Modeling Using Autoregressive Moving Average (ARMA) Models*, Ph.D. Dissertation, Dept. of Engineering Science and Mechanics, Virginia Polytechnic Institute and State University, 1993.
26. Leser, C., Thangjitham, S., Dowling, N. E., "Modeling of Random Vehicle Loading Histories for Fatigue Analysis," *Intl. Journal of Vehicle Design*, Vol. 15, No. 3/4/5, 1994, pp. 467-483.
27. Li, Y. and Kareem, A., "Simulation of Multivariate Nonstationary Random Processes via FFT," *Journal of the Engineering Mechanics Division*, ASCE, Vol. 117, No. 5, May, 1990, pp. 1037-1057.
28. Matsuishi, M. and Endo, T., "Fatigue of Metals Subjected to Varying Stress," Proceedings Japan Society of Mechanical Engineers, Fukuoka, Japan, Mar., 1986.
29. McLean, J. R. and Hoffmann, E. R.. "Analysis of Drivers' Control Movements," *Human Factors*, Vol. 13, No. 5, 1971, pp. 407-418.
30. Mignolet, M. P. and Spanos, P. D., "Simulation of Homogeneous Two-Dimensional Random Fields: Part 1 - AR and ARMA models," *Journal of Applied Mechanics*, Vol. 59, Jun., 1992, pp. S260-S269.
31. Miller, I. and Freund, J. E., *Probability and Statistics for Engineers*, 2nd Edition, Prentice Hall, Englewood Cliffs, 1977.
32. Miner, M. A., "Cumulative Damage in Fatigue," *Journal of Applied Mechanics*, Sep., 1945, pp. A-159-164.
33. Nau. R. F., Oliver, R. M., and Pister, K. S., "Simulating and Analyzing Artificial Nonstationary Earthquake Ground Motions," *Bulletin of the Seismological Society of America*, Vol. 72, Apr., 1982, pp. 615-636.
34. Palmgren, A., *Ball and Roller Engineering*, Translated by G. Palmgren and B. Ruley, SFK Industries, Inc., Philadelphia, 1945, pp. 82-83.
35. Pandit, S. M., *Data Dependent Systems: Modeling Analysis and Optimal Control via Time Series*, Ph.D. Thesis, University of Wisconsin - Madison, 1973.
36. Perret, B., "An Evaluation of a Method for Reconstituting Fatigue Test Loading Sequences from Rainflow Counting," *Proceedings of the 14th ICAF Symposium*, Ottawa, Canada, 1987, pp. 355-401.
37. Priestley, M. B., "Evolutionary Spectra and Nonstationary Processes," *Journal of the Royal Statistical Society*, Series B, Vol. 27, 1965, pp. 204-237.
38. Rice, S. O., "Mathematical Analysis of Random Noise," *Bell System Technical Journal*, Vol. 23, 1944, pp. 232-282.
39. Samaras, E., Shinozuka, M., and Tsurui, A., "ARMA Representation of Random Processes," *Journal of Engineering Mechanics*, ASCE, Vol. 111, No. 3, Mar., 1985, pp. 449-461.
40. Socie, D., "Multiaxial Fatigue Damage Assessment," *Low Cycle Fatigue and Elasto-Plastic Behavior of Materials*, K. -T. Rie, ed., Elsevier, London, 1987, pp. 465-486.
41. Spanos, P. D., "ARMA Algorithms for Ocean Wave Modeling," *Journal of Energy Resources Technology*, Transactions of the ASME, Vol. 105, Sep., 1983, pp. 300-309.
42. Spanos, P. D. and Mignolet, M. P., "ARMA Monte Carlo Simulation in Probabilistic Structural Analysis," *The Shock and Vibration Digest*, Vol. 21, No. 11, 1989, pp. 3-14.
43. ten Have, A. A., "European Approaches in Standard Spectrum Development," *Development of Fatigue Loading Spectra*, *ASTM STP 1006*, J. M. Potter and R. T. Watanabe, eds., American Society for Testing and Materials, 1989, pp. 17-35.
44. Thangjitham, S., Dowling, N. E., Leser, C., "Random Fatigue Load History Reconstruction," *SAE Technical Paper*, 940247, 1994.
45. Theil, H., *Economic Forecasts and Policy*, North-Holland Publishing Company, Amsterdam, 1958.
46. Yang, J.-N., "Simulation of Random Envelope Processes," *Journal of Sound and Vibration*, Vol. 21, 1972, pp. 73-85.